Driven self-assembly of hard nanoplates on soft elastic shells*

Zhang Yao-Yang(章尧旸)[a], Hua Yun-Feng(华昀峰)[b], and Deng Zhen-Yu(邓真渝)[b]†

[a] *Department of Civil Engineering, Tsinghua University, Beijing* 100084, *China*
[b] *Department of Physics, Zhejiang University, Hangzhou* 310027, *China*

(Received 23 March 2015; revised manuscript received 31 May 2015; published online 12 October 2015)

The driven self-assembly behaviors of hard nanoplates on soft elastic shells are investigated by using molecular dynamics (MD) simulation method, and the driven self-assembly structures of adsorbed hard nanoplates depend on the shape of hard nanoplates and the bending energy of soft elastic shells. Three main structures for adsorbed hard nanoplates, including the ordered aggregation structures of hard nanoplates for elastic shells with a moderate bending energy, the collapsed structures for elastic shells with a low bending energy, and the disordered aggregation structures for hard shells, are observed. The self-assembly process of adsorbed hard nanoplates is driven by the surface tension of the elastic shell, and the shape of driven self-assembly structures is determined on the basis of the minimization of the second moment of mass distribution. Meanwhile, the deformations of elastic shells can be controlled by the number of adsorbed rods as well as the length of adsorbed rods. This investigation can help us understand the complexity of the driven self-assembly of hard nanoplates on elastic shells.

Keywords: self-assembly, nanoplate, elastic shell

PACS: 82.35.Np, 82.70.Dd, 82.20.Wt **DOI:** 10.1088/1674-1056/24/11/118202

1. Introduction

Self-assembly behavior has received great attention for potential applications in nanoscience and nanotechnology.[1–8] Aggregation of proteins into functional nanomachines,[9] trimeric proteins into a desired symmetric structure,[10,11] pH-induced self-assembly of peptide-amphiphile into nanofibers,[12] packing of phospholipids into biological membranes,[12] and aggregation of colloidal nanoparticles into crystalline[13] are just a few examples of self-assembly processes. Understanding the physical mechanisms driving self-assembly of biological or artificial components can reveal critical biological processes, and hold promise in the regulation and shaping of nanomaterial in the micrometer range or smaller size.

Elastic surfaces are ubiquitous in nature, and the mechanical properties of these surfaces play an important role both in their biological function and in their wide usage in material engineering.[5] The simplest and most important example of elastic surfaces is biological membrane. The main constituents of biological membranes are phospholipids-amphiphilic molecules, and biological membranes are constantly in contact with various macromolecules that either reside on their surface, or are being transported between the cell and its environment as well as shuffled between different compartments within eukaryotic cells. Since a lipid membrane is only permeable to small uncharged molecules and water, all macromolecules are required to interact with it or cross it. Therefore, self-assembly on biological membranes is an inevitable step in cellular transportation, signaling and recognition.[14] The elastic surface has revolutionized the field of self-assembly by providing a universal mechanism through which arbitrary building blocks can be driven close to each other. The stiffness of an elastic substrate can alter the morphology and dynamics of the tissue cells adhering to it,[15] and there are variable cytoskeleton assembly[16] and cell spreading on substrates of different mechanical properties.[17] Moreover, the surfaces' response to external stress has been exploited in metrology[18,19] and in the production of micro- and nanoscale patterned surfaces that may serve as components with novel optical, electronic and magnetic properties.[20]

The idea of using elastic surfaces as a means of driving self-assembly of arbitrary building blocks was first introduced by Whitesides *et al.*[21] Millimeter-size microchips and micro-components have been successfully self-assembled by manipulating the tension of the interface as well as by tailoring the chemistry of the building blocks.[22] When noninteracting hard particles bind to a deformable elastic shell, some very fantastic phenomena are observed.[3–6,23–25] For example, nanoparticles adhering to the outer surface of an elastic nanotube can self-assemble into linear structures as a result of curvature-mediated interactions.[3] The nontrivial elastic response to deformations of soft elastic surfaces can lead to anisotropic interactions between the nanoparticles resulting in aggregation with different geometrical features, and the morphology of the patterns can be controlled by the mechanical properties of the surface and the strength of the nanoparticle adhesion.[5] Hard nanoparticles binding to a deformable elastic shell can self-assemble into a variety of linear patterns.[6]

Recently, focus has shifted to the development of novel

*Project supported by the National Natural Science Foundation of China (Grant No. 21174131).
†Corresponding author. E-mail: dengbug@gmail.com
© 2015 Chinese Physical Society and IOP Publishing Ltd

fabrication techniques for various shapes, such as cubes, rods, plates and pyramidal particles.[26] In fact, the shape of nanoparticles plays an important role in the self-assembly behaviors. For example, nanocrystals often exhibit well-defined facets that result in a three-dimensional (3D) polyhedral shape or in a polygonal two-dimensional (2D) shape. The self-assembly of such faceted particles enables the formation of highly ordered superlattices, and it is dominated by driving forces that maximize face-to-face contact.[27–29] More recently, a joint experimental-computational multiscale investigation of a class of highly faceted planar lanthanide fluoride nanoplates was performed, and the nanoplates can self-assemble into long-range ordered tilings at the liquid-air interface formed by a hexane wetting layer. The combination of shape-induced entropic and edge-specific energetic effects directs the formation of long-range ordered assemblies,[30] and a series of monodisperse faceted nanocrystals that include circular, rhombic and irregular hexagonal plates, as well as tetragonal bipyramids, are experimentally observed.[30–32] In this paper, we use molecular dynamics (MD) simulation method to study the self-assembly behaviors of nanoplates on elastic shells. As the nanoplate has a two-dimensional structure and the soft elastic shell is also quasi-two-dimensional one, the self-assembly processes of nanoplates on soft elastic shells may be interesting. Understanding the critical physical mechanisms of driving self-assembly will illuminate the key physical processes and simultaneously it is possible to aggregate new materials with novel functional, biochemical and optical properties.

2. Model

As depicted in Fig. 1(a), the elastic surface is modeled by connecting beads into a triangular network.[33,34] To prevent overlap between any two surface monomers, the monomers interact with each other via a purely repulsive truncated and shifted Lennard–Jones potential[6,23,24]

$$U_{\mathrm{LJ}}(r)=\begin{cases}4\varepsilon\left[\left(\frac{\sigma}{r}\right)^{12}-\left(\frac{\sigma}{r}\right)^{6}+\frac{1}{4}\right], & r\le 2^{1/6}\sigma,\\ 0, & r>2^{1/6}\sigma,\end{cases} \tag{1}$$

where r denotes the distance between the centers of two surface monomers, σ is the monomer diameter, and $\varepsilon=1.0k_{\mathrm{B}}T$.

We enforce the elastic surface connectivity by linking adjacent beads via a harmonic spring potential[6]

$$U_{\mathrm{harmonic}}(r)=\frac{K}{2}(r-r_0)^2, \tag{2}$$

where $K=300k_{\mathrm{B}}T/\sigma^2$ is the spring constant, and $r_0=1.23\sigma$ is the equilibrium bond distance.

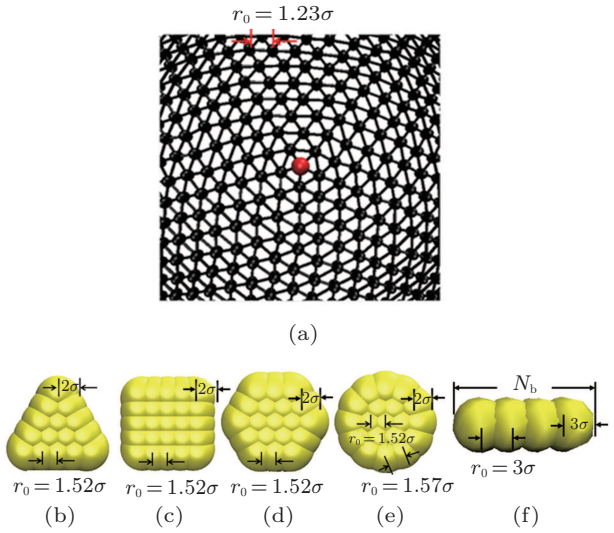


Fig. 1. (color online) (a) Detailed models of hard nanoplates for (b) regular triangle, (c) regular square, (d) regular hexagon, (e) circle and (f) rod; (b)–(f) a fishnet-like network for the elastic surface of shells. Here bond lengths as well as monomer radii are also shown.

The bending rigidity of the elastic surface is modeled by a dihedral potential between adjacent triangles[6,23,24]

$$U_{\mathrm{bending}}=K_{\mathrm{b}}(1+\cos\phi), \tag{3}$$

where ϕ is the dihedral angle between opposite vertices of any two triangles sharing an edge, and K_{b} is the bending energy.

The nanoplates are composed of N_{n} monomers with diameter σ_{C}, which are frozen into rigid-like bodies via the harmonic potential introduced in Eq. (2) with $K'\to K$, $r_0'\to r_0$, and the dihedral potential given in Eq. (3) with $b\to K_{\mathrm{b}}$ and $\theta\to\phi$, where θ is the bond angle between two neighboring bonds. Detailed models of the hard nanoplates are shown in Fig. 1(b). The parameters are $\sigma_{\mathrm{C}}=4\sigma$ except that $\sigma_{\mathrm{C}}=6\sigma$ for the rods, $K'=1000k_{\mathrm{B}}T/\sigma^2$, $r_0'=0.38\sigma_{\mathrm{C}}$, and $b=10000k_{\mathrm{B}}T$ to minimize possible deformation of the hard plates. For regular triangle ($N_{\mathrm{n}}=15$) and hexagon ($N_{\mathrm{n}}=19$), monomers are arranged on a two-dimensional hexagonal lattice; for regular square ($N_{\mathrm{n}}=25$), monomers are arranged on a two-dimensional simple cubic (SC) lattice, while for rods, monomers are connected by N_{n} monomers into a 1D "stick". In order to maintain stability, the neighboring monomers are partially overlapped. Meanwhile, monomers between any two different nanoplates interact with each other via the L–J potential described in Eq. (1), and the plate–plate interaction is short-ranged repulsive.

The generic binding of the monomer of nanoplates to the elastic shell is described by a Morse potential[23,24]

$$U_{\mathrm{Morse}}(r)=\begin{cases}D_0(\mathrm{e}^{-2\alpha(r-r_{\mathrm{M}})}-2\mathrm{e}^{-\alpha(r-r_{\mathrm{M}})}), & r\le 10\sigma,\\ 0, & r>10\sigma,\end{cases} \tag{4}$$

where r is the center-to-center distance between a nanoplate monomer and a surface monomer, $D_0=8.0k_{\mathrm{B}}T$ is the binding energy, $r_{\mathrm{M}}=2.5\sigma$ is the monomer-bead contact distance, and

$\alpha = 1.25/\sigma$. Our aim of this paper is to investigate the self-assembly of nanoplates on an elastic shell, strong attractive interactions have to be considered. For a very weak binding energy, there is almost no interaction between the nanoplates and the shell, and the nanoplates are located randomly in the box, known as the gas phase.[25] At a moderate binding energy, the nanoplates are uniformly adsorbed on the shell, and there are no self-assembly structures for nanoplates.[25] Although a weak or moderate binding energy has an important influence in the self-assembly behavior, there are no self-assembly structures for nanoplates at a weak or moderate binding energy. Therefore, only at a large enough binding energy, one can observe the driven self-assembly behaviors for nanoplates on elastic shells.

We employ the LAMMPS molecular dynamics package[35] with a Nose–Hoover thermostat[36,37] in the *NVT* ensemble to study the driven self-assembly behavior of nanoplates on soft elastic shells. The temperature of the system is set to $T = 1.0$, the time step is $\tau = 0.001\tau_0$, and each simulation runs at least 2×10^7 steps in the periodic box $200\sigma \times 200\sigma \times 200\sigma$. Meanwhile, the number of the surface monomers is $N_s = 10242$, and the radius of elastic shell is $R = 32.5\sigma$.

3. Results and discussion

3.1. Ordered structures of adsorbed hard nanoplates on elastic shells

A dimensionless parameter known as the Föppl–von Kàrmàn number $\gamma = YR^2/K_b$ can well describe the surface tension of elastic shells, where Y is the Young's modulus of the elastic shell and K_b is the bending rigidity defined in the continuum theory of elasticity.[38] Since the Young's modulus of the elastic shell Y and the shell radius R in our model are constant, the Föppl–von Kàrmàn number is simplified as $\gamma \propto 1/K_b$. Therefore, the elastic property of the shell can be illustrated by the bending energy K_b. The driven self-assembly behaviors of hard nanoplates on soft elastic shells depend on the shape of hard nanoplates, the bending energy of elastic shells, and the number of hard nanoplates. A series of simulations for various shapes of nanoplates (regular triangle, square, regular hexagon, circle, and short rod with 4 monomers) with different nanoplate numbers $N = 36$, 48, and 60 are carried out, and the results are shown in Fig. 2. For the elastic shell with a moderate bending energy ($K_b = 10000$), the nanoplates aggregate in the flat regions, and the ordered structures of aggregation nanoplates are observed. The structure of each aggregated cluster is governed by the shape of nanoplates and the number of nanoplates in the system, while the total number of the aggregation clusters is always a constant of 12. According to previous work, for an elastic shell with a weak bending energy of $K_b = 1000$, there are a series of peaks on the $\Theta\Phi$ surface in the spherical coordinate system, and the area of each peak and the distance between any two neighboring peaks are identical, and the number of peaks is twelve.[23,25] There are twelve required five-fold disclinations due to the topology of the discrete spherical model, which has been proved in previous works.[39,40] However, for the elastic shell with a relatively high bending energy of $K_b = 10000$, which is larger than the stretching energy,[6] the shape of the elastic shell is mainly determined by the bending energy and the radius distributions of the elastic shell on the $\Theta\Phi$ surface. The $\Theta\Phi$ surface of the shell with $K_b = 10000$ is completely different from that of the shell with $K_b = 1000$.[23] The peak regions in the radius distributions of the elastic shell with a weak bending energy become the valley regions for the elastic shell with a high bending energy.[23] The aggregation clusters of hard nanoplates are distributed among these 12 regions. For nanoplates with the fixed shape, the aggregation structure depends mainly on the total number of nanoplates in the simulation system. For example, for square nanoplates, there are three different aggregation structures for $N = 36$, in which two, three, and four squares are aggregated, while six, seven, and eight squares are aggregated for $N = 60$.

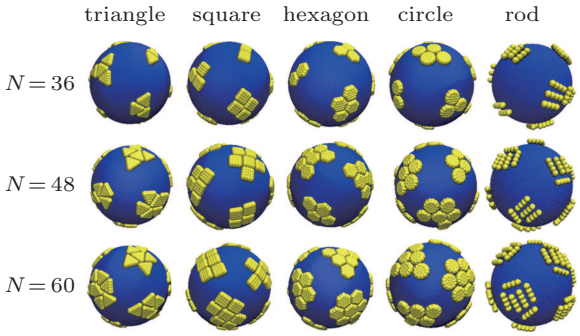


Fig. 2. (color online) Simulation snapshots of representative aggregation structures for regular triangle, regular square, regular hexagon, circle, and rod with various numbers of hard nanoplates $N = 36$, 48, and 60, respectively. Here the bending energy of the elastic shell is $K_b = 10000$, and N is the total number of hard nanoplates.

Detailed descriptions of the ordered structures are given in Fig. 3. For each n, there are various aggregation structures, where n is the number of nanoplates in one aggregation cluster. For a large n, there are different conformations for a given n, and the percentage of different conformations is shown in the top right corner of the snapshots. Hard nanoplates are aggregated on elastic shells on the basis of the minimization of the second moment of the mass distribution.[41,42] As there exist some plate regions in the radius distributions on the $\Theta\Phi$ surface,[23] hard nanoplates are aggregated on these regions as compactly as possible. For regular triangles, the aggregated structures are not perfect and the triangle edges are not parallel to each other completely for $n = 6$, 7. However, regular triangles are aggregated in a perfect manner for $n = 2$, 3, and 4. For regular squares, most of the squares are in the parallel arrangement, and some squares can move randomly along the

parallel edges. For regular hexagons and circles, the perfectly aggregated structures are shown in Fig. 3.

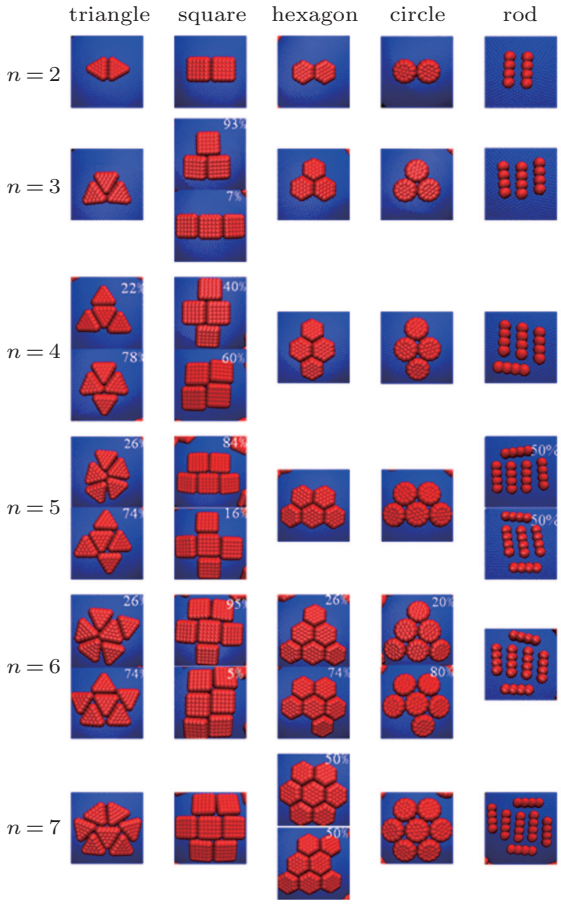


Fig. 3. (color online) Some representative conformations of hard nanoplates on the soft elastic shells with various n at $K_b = 10000$. Here $n$is the number of nanoplates in one aggregation cluster, and the percentage of different configurations is shown in the top right corner of the snapshot.

To understand the mechanism of forming the ordered aggregation structures, we choose the regular hexagons as an example to explore the simulation process of a system with a constant bending energy $K_b = 10000$, and the results are shown in Fig. 4. Initially, the nanoplates are placed randomly in the simulation box and away from the elastic shell. The radius distribution on the $\Theta\Phi$ surface for the elastic shell is uniform, and the radial distances of the surface monomers are almost close to 32.5σ for all surface monomers. After a short simulation time, the nanoplates are adsorbed on the elastic shell under the effects of binding energy, which makes the shells fluctuate drastically and leads to a decrease of the mean radius of elastic shells from $\langle R\rangle = 32.5$ at $t = 0$ to $\langle R\rangle = 31.4$ at $t = 10^4\tau$ due to the compression of adsorbed nanoplates on the elastic shells. The surface tension of the elastic shell can drive the nanoplates to move towards the flat regions of the elastic shells and these movements can minimize the total system energy, see Fig. 4(c2). After a long period of equilibrium, ordered

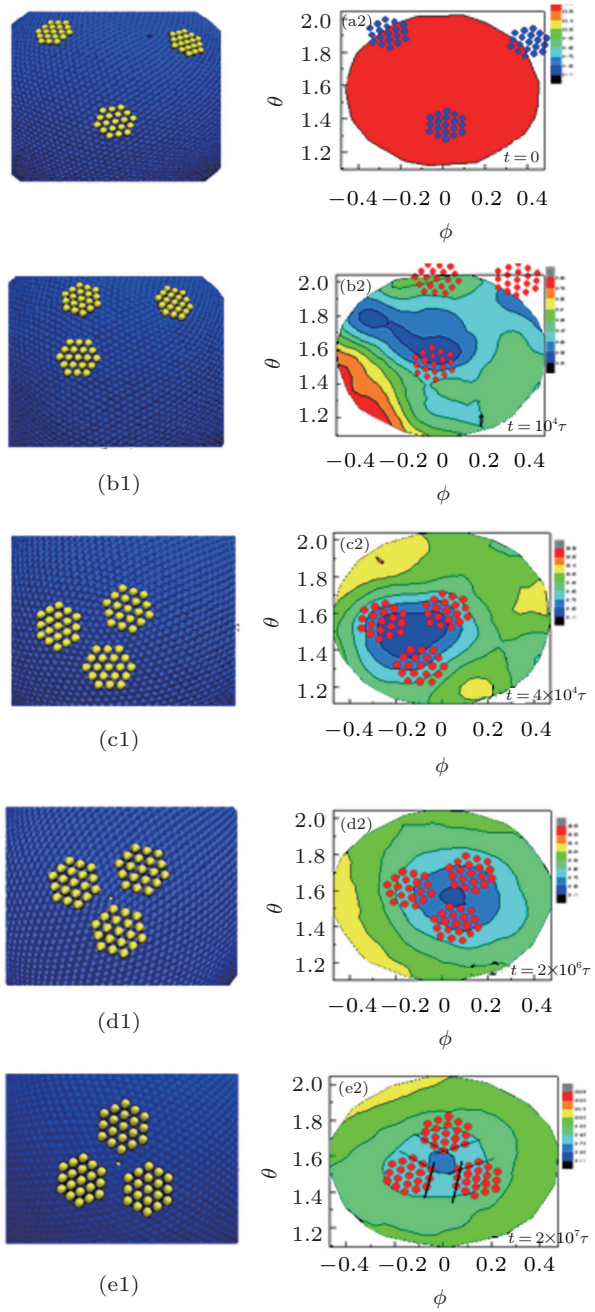


Fig. 4. (color online) Left: Snapshots at different simulation times suggesting that the combination of nanoplate shape and surface tension of soft shell directs the formation of an ordered structure for regular hexagon. Right: The corresponding radius distributions of elastic shells at different simulation times.

structures of nanoplates are finally formed, in which the adjacent hexagon edges are parallel to each other because this parallel arrangement can maximize the local packing fraction, see Fig. 4(e2). Therefore, we can conclude that the driven self-assembly behavior of the hard nanoplates consists of two stages: firstly, nanoplates are adsorbed onto the shell randomly and then accumulate towards the center of the flat region driven by the surface tension of the elastic shell; secondly, the nanoplates rearrange on the basis of the maximization of local packing fraction. To explain the process of self-assembly behavior more intuitively, we draw schematic illustrations about

the aggregation mechanism in Fig. 5. When nanoplates are adsorbed on the surface of the elastic shell, the shell surface has an obvious deformation and there are some valley regions on the surface of elastic shells. If the nanoplates are adsorbed on these valley regions, the nanoplates move towards the center of the valley regions, see Fig. 5(a). After the nanoplates are driven by the surface tension, the nanoplates approach each other, and they are arranged on the basis of maximization of local packing fraction and the parallel arrangement of nanoplate edges, see Fig. 5(b). This is the mechanism of forming ordered structures for nanoplates on elastic shells.

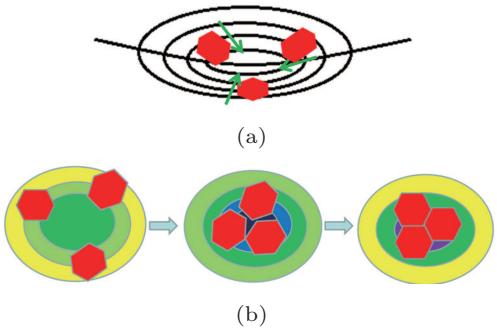


Fig. 5. (color online) Schematic illustrations indicating that the driven self-assembly behaviors of the hard nanoplates consist of two stages: (a) the nanoplates are adsorbed onto the shell randomly and then accumulate towards the center of the flat region driven by surface tension of the elastic shell; (b) the nanoplates rearrange on the basis of the maximization of local packing fraction.

In order to explore whether nanoplates are driven to flat regions or flat regions are induced by aggregated plates in more detail, we calculate the energy distribution of the elastic shell for $N = 0$, 12, and 36, as shown in Fig. 6. It can be concluded that the adsorption behaviors depend mainly on the bending energy of the elastic shells because all the regular hexagons are located at the regions with the low bending energies. The nanoplates are aggregated on the basis of the minimization of the second moment of the mass distribution.[41,42] The driving force for nanoplates to be aggregated comes from the surface tension of elastic shells because there are no interactions between the nanoplates.

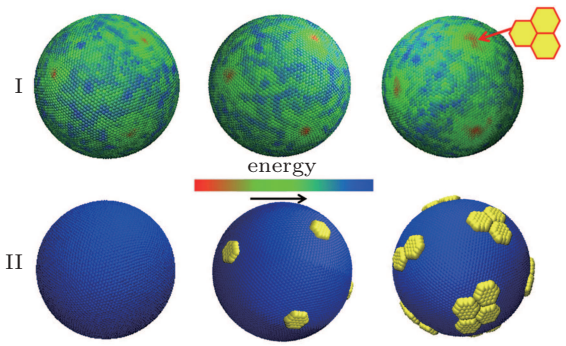


Fig. 6. (color online) The energy distribution of the soft elastic shell (first row) and the corresponding snapshots (second row) for regular hexagons with $N = 0$, 12, and 36.

3.2. Effects of bending energy on driven self-assembly behaviors of adsorbed nanoplates

In order to investigate the effects of bending energy K_b on the driven self-assembly behaviors of nanoplates on elastic shells, a series of simulations with various bending energies for $K_b = 100$, 10000, and 5×10^5 are performed, and the results are shown in Fig. 7. For the elastic shell with a very low bending energy of $K_b = 100$, it is collapsed completely no matter what shape the nanoplate is. For the elastic shell with a moderate bending energy of $K_b = 10000$, the aggregation structures of nanoplates are distributed among the relatively flat regions. For the elastic shell with a very high bending energy (such as 5×10^5), it needs a very large energy for the shells to deform a little, and the adsorption behavior of nanoplates on the shells is isotropic. The driven self-assembly process cannot occur for $K_b = 5 \times 10^5$, and no aggregation cluster for nanoplates can be formed, see Fig. 7(c). In fact, the adsorption behaviors of nanoplates on elastic shells are quasi-dimensional. In order to compare the different adsorption behaviors of nanoplates on elastic shells with those on a two-dimensional (2D) surface, we also simulate the adsorption processes of nanoplates on two-dimensional surfaces, and the results are also shown in Fig. 7(d). The nanoplates are adsorbed randomly on a two-dimensional surface, and no aggregation clusters are formed. Therefore, the adsorption behaviors of nanoplates on soft elastic shells are completely different from those on two-dimensional surfaces.

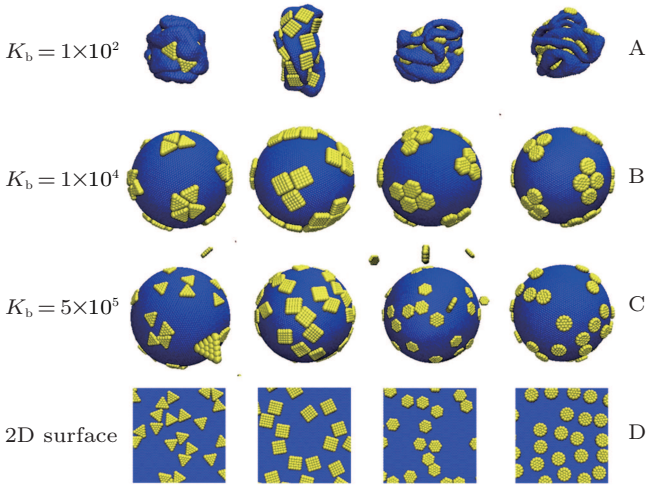


Fig. 7. (color online) Evolutions of hard nanoplates on soft elastic shells at various bending energies with $K_b = 100$ (A), 10000 (B), and 5×10^5 (C) for regular triangle, square, hexagon, and circle, respectively. The adsorption behaviors of hard nanoplates on two-dimensional (2D) planes are shown in panel (D) for comparison. Here $N = 48$.

To gain insight into the physical origin of different aggregation behaviors for nanoplates on elastic shells with different bending energies, we plot three possible schematic illustrations in Fig. 8. For a very soft elastic shell, the shell is so soft that the nanoplates can affect the shapes of shells seriously, and the collapsed structures are observed, see Fig. 8(a). For the elastic shell with moderate bending energy, as there are some

flat regions on the elastic surface, several nanoplates can be aggregated on the plate regions of the elastic surface. As the shell surface is relatively soft, the elastic shell can deform a little according to the interactions between the nanoplates and the elastic shells. However, for elastic shell with a very high bending energy, the attraction ability of hard shell for nanoplates may decrease because some monomers for nanoplates exceed the attraction ranges, see the inset of Fig. 8(c). In fact, the adsorption abilities of nanoplates on the hard shells are weaker than those on the elastic shells at the same binding energy. Meanwhile, the adsorption process onto the soft elastic shells for nanoplates includes two stages: i) the nanoplates are adsorbed on the shells randomly; ii) the nanoplates are rearranged on the basis of the maximization of local packing fraction. However, for the very hard shells, the adsorption process of the nanoplates on the hard shells only consists of the first stage. Therefore, the effects of bending energy on driven self-assembly behaviors of adsorbed nanoplates are obvious, and the adsorption behaviors of nanoplates on elastic shells have their distinguishing features.

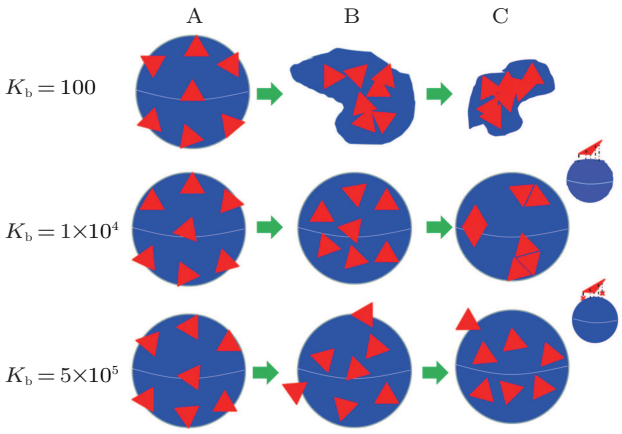


Fig. 8. (color online) Schematic illustrations showing the effects of bending energy on the driven self-assembly behaviors of regular triangle on soft elastic shells. A: Nanoplates are located randomly in the simulation box; B: nanoplates are adsorbed onto the shell; C: the whole system reaches equilibrium. Different attractive abilities of soft elastic shells and hard shells for regular triangles are given in the top right corner, and the cross means that the shell monomer and the regular triangle monomer are hardly attractive to each other.

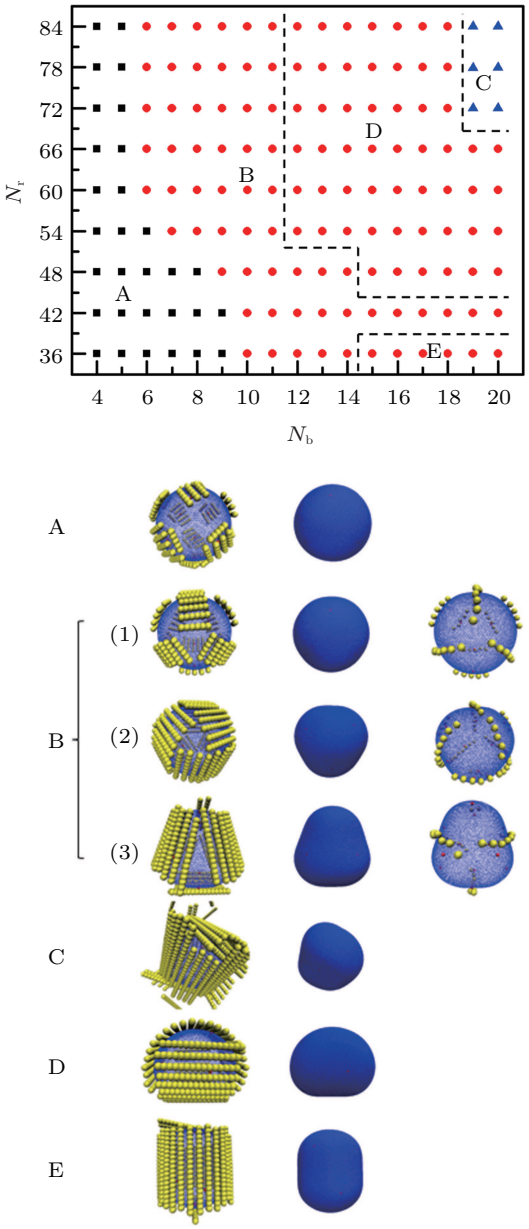


Fig. 9. (color online) Phase diagram of aggregation structures for rods on elastic shell in the plane of rod length N_b and the number of rods N. There are three main phases: 12-cluster (A, black square), $(3+n)$-cluster (B, red circle), irregular (C, blue triangle). Additionally, two possible phases are hidden in the above phases and labeled by dashed lines, and they are 2-cluster (D), 1-cluster (E). Typical snapshots are: A phase with $N = 66$, $N_b = 5$; B phase with $N = 66$, $N_b = 6$ B(1); $N = 66$, $N_b = 9$ B(2); $N = 42$, $N_b = 15$ B(3); C phase with $N = 78$, $N_b = 20$; D phase with $N = 48$, $N_b = 15$; and E phase $N = 36$, $N_b = 18$.

3.3. Deformations of elastic shell controlled by adsorbed rods

Rods have a special property of additional orientation entropy, which is different from the normal nanoplates. Previous simulations on the aggregation behaviors of short and long rods on soft elastic shells have found that the aggregation structure of the rods is relevant to the bending energy of the elastic shell.[24] However, the detailed discussion about the dependences of rod lengths and the number of rods has not been given yet. Figure 9 shows the phase diagram in the N_b–N plane. Here N_b is the number of monomers in a rod, and N is the number of rods in our simulation system. For short rods (i.e., $N_b \leq 9$), the rods are aggregated and can form 12 clusters in the 12 flat regions as mentioned above, while the shell maintains its original shape as a sphere (see phase A in Fig. 9). When the rod length increases, due to the parallel arrangement of the rods, some flat regions can no longer hold enough rods, so that some clusters tend to connect to each other and form some larger clusters, and a transition from A phase to B phase occurs. B phase consists of 3 large clusters and several small clusters. Three large clusters pinch the shell and the shell is

deformed into a tricorn. Some small clusters are aggregated in the empty flat regions, and the number of small clusters decreases with the increase of rod length. The number of large clusters is 3, and the numbers of small clusters are 6, 3, and 1 in Figs. 9(b1), 9(b2), and 9(b3). For simplicity, we group them into phase B. For long rods ($N_b \geq 15$) with $N = 36$, the rods can squeeze the shell into an ellipsoid, and form a large circular cluster surrounding the shell surface (see phase D in Fig. 9). For a sufficient number of long rods, such as $N_b \geq 12$ and $N \geq 54$, or $N_b \geq 15$ and $N = 48$, a two-cluster phase is observed, in which the rods nearly cover the entire surface of the shell, and the shell deforms like a pillow (see phase E in Fig. 9). If the number of long rods is greater than 68, although the adsorbed rods are locally parallel to each other, they have no space to adjust their positions on the shell, and the shell deforms irregularly (see phase C in Fig. 9).

We calculate the surface asphericity A of the shell, which is defined as[6,23]

$$A = \frac{\langle \Delta R^2 \rangle}{\langle R \rangle^2} = \sum_{i=1}^{N_S} \frac{(R_i - \langle R \rangle)^2}{\langle R \rangle^2}, \tag{5}$$

where R_i is the radial distance of the surface monomer i, and $\langle R \rangle$ is the mean radius of the elastic shell. Figure 10 shows that the asphericity of the shell increases slowly for short adsorbed rods with $N_b \leq 8$, followed by a rapid growth for the moderate lengths of rods with $9 \leq N_b \leq 15$, and slows down a little with $N_b \geq 16$. One notes that for long rods, the larger number of rods the system consists of, the smaller the asphericity A is. For short rods, the elastic shell does not undergo large deformations to ensure the rod–shell interactions to minimize total energy, so that the original spherical shape of the shell is well maintained. When the rod length increases, the binding energy causes remarkable deformations of the shell, followed by the self-assembly behaviors of the long rods. Governed by the orientational entropy, these rods rearrange themselves and affect the shape of the shells in return. Finally, one can obtain various shapes of shells such as a tricorn, an ellipsoid, or a pillow-like shape. However, for a number of long rods in the system, the adsorption behaviors of the rods are isotropic, and there is not enough space to adjust their positions. The shell has to accommodate and deform irregularly, so we can observe a slight decay on the curve for large N_b, see Fig. 10. The potential interactions dominate the deformation of the elastic shell and the driven self-assembly behavior of rods depends on the competition between the orientational entropy of rods and the potential interactions of elastic shell.

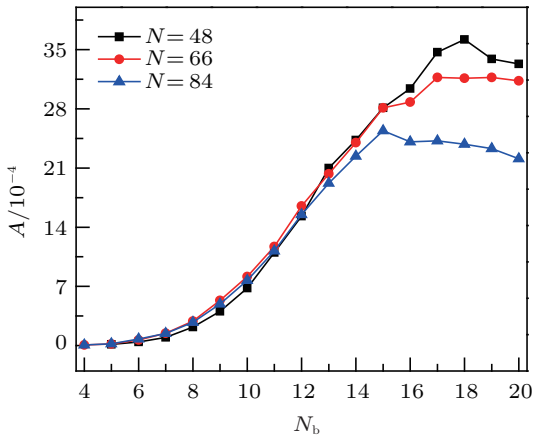


Fig. 10. (color online) The surface asphericity of elastic shell A as a function of rod length N_b for various numbers of nanorods.

4. Conclusions

In this paper, we investigate the driven self-assembly behaviors of hard nanoplates on soft elastic shells by employing a molecular dynamics simulation method. The adsorption behaviors of nanoplates on elastic shell depend mainly on the bending energy of the elastic shell. The driven self-assembly structures of adsorbed nanoplates are determined by the minimization of the second moment of the mass distribution. For shells with a low bending energy, the elastic shells are completely collapsed. For shells with a moderate bending energy, ordered structures are formed for various shapes of hard nanoplates. For shells with a high bending energy, the nanoplates are adsorbed randomly on the shell. The shell is hardly deformed for triangles, squares, hexagons, circles, and short rods, and has a remarkable deformation for long rods because of the large binding energy caused by the rod–shell interactions. One can observe various shapes of shells such as a sphere, a tricorn, an ellipsoid, and a pillow-like shape by adjusting the number of rods and the rod lengths. These investigations can help us understand the complexity of driven self-assembly of hard nanoplates on elastic shells and can hold promise for the applications in material designing as well as controlling the shape of shells in the micrometer range or smaller sizes.

References

[1] Zhang S M, Greefield M A, Mata A, Palmer L C, Bitton R, Mantei J R, Aparicio C, Olvera de Cruz M and Stupp S I 2010 *Nat. Mater.* **9** 594
[2] Vernizzi G, Sknepnek R and Olvera de Cruz M 2011 *Proc. Natl. Acad. Sci. USA* **108** 4292
[3] Pàmies J C and Cacciuto A 2011 *Phys. Rev. Lett.* **106** 045702
[4] Šarić A and Cacciuto A 2012 *Phys. Rev. Lett.* **108** 118101
[5] Šarić A and Cacciuto A 2011 *Soft Matter* **7** 8324
[6] Šarić A and Cacciuto A 2011 *Soft Matter* **7** 1874
[7] Jha P K, Kuzovkov V, Grzybowski B A and Olvera de Cruz M 2012 *Soft Matter* **8** 227
[8] Velichko Y S and Olvera de Cruz M 2006 *J. Chem. Phys.* **124** 214705
[9] Alberts B, Johnson A, Lewis J, Raff M, Roberts K and Wzlter P 2008 *Molecular Biology of* **the** Cell (New York: Garland Science)
[10] Rothemund P W K 2006 *Nature* **440** 297
[11] King N P, Sheffler W, Sawaya M R, Vollmar B S, Sumida J P, Andre I, Gonen T, Yeates T O and Baker D 2012 *Science* **336** 1171
[12] Hartgerink J D, Beniash E and Stupp S I 2001 *Science* **294** 1684
[13] Nykypanchuk D, Maye M M, Lelie D V D and Gang O 2008 *Nature* **451** 549

[14] Brown F L H 2008 *Annu. Rev. Phys. Chem.* **59** 685
[15] Discher D E, Janmey P and Wang Y 2005 *Science* **310** 1139
[16] Engler A, Bacakova L, Newman C, Hategan A, Griffin M and Discher D 2004 *Biophys. J.* **86** 617
[17] Georges P C and Janmey P A 2005 *J. Appl. Physiol.* **98** 1547
[18] Huang J, Juszkiewicz M, de Jeu W H, Cerda E, Emrick T, Menon N and Russell T P 2007 *Science* **317** 650
[19] Stafford C M, Harrison C, Beers K L, Karim A, Amis E J, Vanlandingham M R, Kim H C, Volksen W, Miller R D and Simony E E 2004 *Nat. Mater.* **3** 545
[20] Schweikart A, Fortini A, Wittemann A, Schmidt M and Fery A 2010 *Soft Matter* **6** 5860
[21] Boncheva M and Whitesides G M 2005 *MRS Bull* **30** 736
[22] Xiong X and Hanein Y 2003 *J. Microelectromech. Syst.* **12** 117
[23] Zhang D, Chai A H, Wen X H, He L L, Zhang L X and Liang H J 2012 *Soft Matter* **8** 2152
[24] Wen X H, Zhang D, Chai A H, He L L, Ran S Y and Zhang L X 2012 *Soft Matter* **8** 6706
[25] Jiang Y W, Zhang D, Jin Y K and Zhang L X 2013 *J. Chem. Phys.* **138** 214901
[26] Zhang S Z, Kou X S, Yang Z, Shi Q H, Stucky G D, Sun L D, Wang J F and Yan C H 2007 *Chem. Commun.* **18** 1816
[27] Shevchenko E V, Talapin D V, Kotov N A, Brien S O and Murray C B 2006 *Nature* **439** 55
[28] Yethiraj A and Van Blaaderen A 2003 *Nature* **421** 513
[29] Chen Q, Bae S C and Granick S 2011 *Nature* **469** 381
[30] Ye X C, Chen J, Engel M, Millan J A, Li W B, Qi L, Xing G Z, Collins J E, Kagan C R, Li J, Glotzer S C and Murray C B 2013 *Nat. Chem.* **5** 466
[31] Zhang Y W, Sun X, Si R, You L PN and Yan C H 2005 *J. Am. Chem. Soc.* **127** 3260
[32] Wang F, Han Y, Lim C S, Lu Y, Wang J, Xu J, Chen H, Hong M and Liu X 2010 *Nature* **463** 1061
[33] Hsu C W and Chen Y L 2010 *J. Chem. Phys.* **133** 034906
[34] Lidmar J, Mirny L and Nelson D R 2003 *Phys. Rev. E* **68** 051910
[35] Plimpton S J 1995 *J. Comput. Phys.* **117** 1
[36] Nose S 1984 *J. Chem. Phys.* **81** 511
[37] Hoover W G 1985 *Phys. Rev. A* **31** 1695
[38] Landau L D and Lifshitz E M 1970 *Theory of Elasticity* (New York: Pergamob)
[39] Bowick M J and Sknepnek R 2013 *Soft Matter* **9** 8088
[40] Funkhouser C M, Sknepnek R and Olvera de Cruz M 2013 *Soft Matter* **9** 60
[41] Manoharam V N, Elsesser M T and Pine D J 2003 *Science* **301** 483
[42] Graham R L and Sloane N J A 1990 *Discrete Comput. Geom.* **5** 1